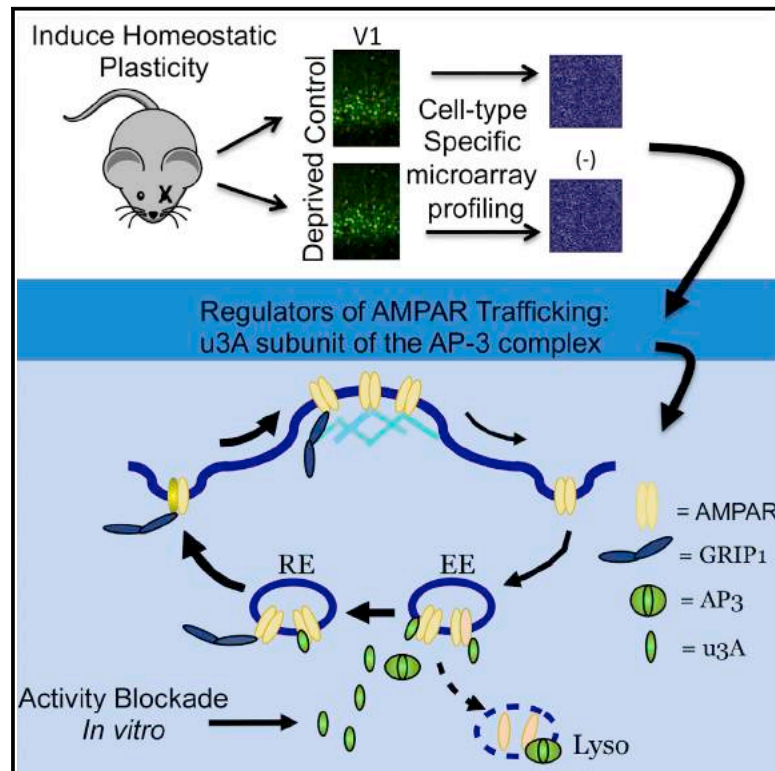


# Cell Reports

## Upregulation of $\mu$ 3A Drives Homeostatic Plasticity by Rerouting AMPAR into the Recycling Endosomal Pathway

### Graphical Abstract



### Authors

Celine C. Steinmetz,  
Vedakumar Tatavarty, Ken Sugino, ...,  
Suzanne Paradis, Sacha B. Nelson,  
Gina G. Turrigiano

### Correspondence

nelson@brandeis.edu (S.B.N.),  
turrigiano@brandeis.edu (G.G.T.)

### In Brief

How the abundance of synaptic receptors is controlled during synaptic plasticity is poorly understood. Here, Steinmetz et al. identify activity-dependent upregulation of the  $\mu$ 3A subunit of AP-3 as a trafficking “switch point” that reroutes AMPA-type glutamate receptors from the lysosomal to the recycling endosomal pathway to enhance synaptic strength.

### Highlights

- Cell-type-specific screen identifies transcripts involved in homeostatic synaptic scaling
- $\mu$ 3A is identified as a critical “switch point” in AMPAR trafficking
- Upregulation of  $\mu$ 3A reroutes AMPAR into the recycling pathway to induce plasticity

### Accession Numbers

GSE56758



# Upregulation of $\mu$ 3A Drives Homeostatic Plasticity by Rerouting AMPAR into the Recycling Endosomal Pathway

Celine C. Steinmetz,<sup>1,3</sup> Vedakumar Tatavarty,<sup>1</sup> Ken Sugino,<sup>1,4</sup> Yasuyuki Shima,<sup>1</sup> Anne Joseph,<sup>1</sup> Heather Lin,<sup>1</sup> Michael Rutlin,<sup>1,5</sup> Mary Lambo,<sup>2</sup> Chris M. Hempel,<sup>1,6</sup> Benjamin W. Okaty,<sup>1,7</sup> Suzanne Paradis,<sup>1</sup> Sacha B. Nelson,<sup>1,\*</sup> and Gina G. Turrigiano<sup>1,8,\*</sup>

<sup>1</sup>Department of Biology and Center for Behavioral Genomics, Brandeis University, Waltham, MA 02454, USA

<sup>2</sup>Department of Brain and Cognitive Science, MIT, Cambridge, MA 02139, USA

<sup>3</sup>Present address: Novartis Pharma, Basel 4002, Switzerland

<sup>4</sup>Present address: Janelia Farm Research Campus, Howard Hughes Medical Institute, Ashburn, VA 20147, USA

<sup>5</sup>Present address: Department of Biochemistry and Molecular Biophysics, HHMI, Columbia College of Physicians and Surgeons, Columbia University, New York, NY 10032, USA

<sup>6</sup>Present address: Galenea Corporation, Cambridge, MA 02139, USA

<sup>7</sup>Present address: Department of Genetics, Harvard Medical School, Boston, MA 02115, USA

<sup>8</sup>Lead Contact

\*Correspondence: [nelson@brandeis.edu](mailto:nelson@brandeis.edu) (S.B.N.), [turrigiano@brandeis.edu](mailto:turrigiano@brandeis.edu) (G.G.T.)

<http://dx.doi.org/10.1016/j.celrep.2016.08.009>

## SUMMARY

Synaptic scaling is a form of homeostatic plasticity driven by transcription-dependent changes in AMPA-type glutamate receptor (AMPA) trafficking. To uncover the pathways involved, we performed a cell-type-specific screen for transcripts persistently altered during scaling, which identified the  $\mu$  subunit ( $\mu$ 3A) of the adaptor protein complex AP-3A. Synaptic scaling increased  $\mu$ 3A (but not other AP-3 subunits) in pyramidal neurons and redistributed dendritic  $\mu$ 3A and AMPAR to recycling endosomes (REs). Knockdown of  $\mu$ 3A prevented synaptic scaling and this redistribution, while overexpression (OE) of full-length  $\mu$ 3A or a truncated  $\mu$ 3A that cannot interact with the AP-3A complex was sufficient to drive AMPAR to REs. Finally, OE of  $\mu$ 3A acted synergistically with GRIP1 to recruit AMPAR to the dendritic membrane. These data suggest that excess  $\mu$ 3A acts independently of the AP-3A complex to reroute AMPAR to RE, generating a reservoir of receptors essential for the regulated recruitment to the synaptic membrane during scaling up.

## INTRODUCTION

The ability of networks to maintain stable function over time, and to efficiently store information, is thought to rely on homeostatic plasticity mechanisms that stabilize neuronal and network activity (Davis, 2013; Turrigiano and Nelson, 2004). Synaptic scaling is a form of homeostatic plasticity that scales postsynaptic strength up or down in response to perturbations in neuronal firing (Gainey et al., 2009, 2015; Goold and Nicoll,

2010; Ibata et al., 2008), a process thought to contribute to the stabilization of firing rates both in vitro (Turrigiano et al., 1998) and in vivo (Hengen et al., 2013, 2016). Synaptic scaling is accomplished through changes in the abundance of postsynaptic AMPA receptors (AMPA), but despite great effort, the full set of molecular trafficking events that homeostatically adjust synaptic AMPAR abundance is poorly understood (Poza and Goda, 2010; Turrigiano, 2012). In particular, although synaptic scaling is known to be transcription dependent (Gainey et al., 2015; Goold and Nicoll, 2010; Ibata et al., 2008; Meadows et al., 2015), the factor or factors that are transcriptionally regulated to drive synaptic scaling are largely unknown. We thus set out to devise an unbiased screen for factors that are persistently upregulated during synaptic scaling in the hopes of gaining deeper insight into the transcription-dependent AMPAR trafficking pathways involved in this critical form of synaptic plasticity.

Synaptic scaling up is induced within primary visual cortex (V1) by brief sensory deprivation (Desai et al., 2002; Lambo and Turrigiano, 2013). Several studies have examined the transcriptional changes within extracts of V1 following visual deprivation protocols (Lachance and Chaudhuri, 2004; Majdan and Shatz, 2006; Tropea et al., 2006). However, these earlier studies probed tissue derived from total V1, including all cell types and all layers. This is problematic, because synaptic scaling is expressed in a cell-type- and layer-specific manner (Desai et al., 2002; Maffei and Turrigiano, 2008); therefore, this approach does not provide the necessary sensitivity to isolate transcripts that are specifically involved in synaptic scaling. For this reason, we designed a screen that would allow us to probe for transcriptional changes in a defined population of pyramidal neurons in which we know synaptic scaling is induced. Two days of visual deprivation via intraocular tetrodotoxin (TTX) injection induces synaptic scaling up of miniature excitatory postsynaptic currents (mEPSCs) onto layer 4 (L4) star pyramidal neurons in rodent



visual cortex during early postnatal development (Desai et al., 2002). Here we generated a mouse with mCitrine expressed within these L4 star pyramids, allowing us to probe for transcriptional changes in this specific cell population (Sugino et al., 2006). This highly targeted approach revealed a relatively small number of transcripts (30) with expression changes that reached the criterion (fold change > 1.5,  $p < 0.0034$ ) following visual deprivation.

Surprisingly, two of these, *Ap3m1* and *Ap4m*, code for  $\mu$  subunits ( $\mu3A$  and  $\mu4$ , respectively) of the heterotetrameric clathrin adaptor protein (APC) complexes AP-3 and AP-4. The APC family is composed of five members (AP-1 through AP-5) that sort and shuttle membrane-bound cargo between different endosomal and cell-surface compartments (Faúndez et al., 1998; Hirst et al., 2013; Le Borgne et al., 1998; Nakatsu and Ohno, 2003; Newell-Litwa et al., 2007; Robinson and Bonifacino, 2001; Simpson et al., 1997); the  $\mu$  subunits are critical for most cargo recognition (Bonifacino and Traub, 2003; Mardones et al., 2013; Ohno et al., 1998; Traub and Bonifacino, 2013). Although none of these complexes were previously known to have activity-regulated expression, several of them have been implicated in basal sorting and trafficking of glutamate receptors (Margeta et al., 2009; Kastning et al., 2007; Lee et al., 2002). In particular,  $\mu3A$  and  $\mu4$  can bind AMPAR indirectly through interactions with transmembrane AMPR regulatory proteins (TARPs) (Matsuda et al., 2008, 2013), and this interaction is important for dendritic trafficking of AMPAR (Matsuda et al., 2008) and for N-methyl-D-aspartate (NMDA)-induced trafficking of internalized AMPAR from early endosomes (EEs) to lysosomes (AP-3; Matsuda et al., 2013). These considerations suggest that  $\mu3A$  could contribute to the regulated trafficking of AMPAR that underlies synaptic scaling up (Kennedy and Ehlers, 2006; Turrigiano, 2008).

Here we show that  $\mu3A$  upregulation plays an essential role in synaptic scaling up by trafficking GluA2-containing AMPAR into the recycling pathway. AP-3 is classically known for sorting membrane proteins into the lysosomal pathway for degradation (Bonifacino and Traub, 2003), so it was surprising to find that TTX treatment rerouted  $\mu3A$  from lysosomes to recycling endosomes (REs). Both TTX treatment and overexpression (OE) of  $\mu3A$  were able to drive AMPAR into the RE pathway, as was OE of a truncated  $\mu3A$  that cannot interact with the rest of the AP-3 complex (Mardones et al., 2013). Furthermore, knockdown (KD) of  $\mu3A$ , which blocks the normal increase in  $\mu3A$  induced by activity blockade, prevented the activity-dependent rerouting AMPAR to REs and blocked synaptic scaling. Finally, OE of  $\mu3A$  acted synergistically with the GluA2 trafficking protein GRIP1 to recruit AMPAR to the dendritic surface. Taken together, these data show that activity blockade transcriptionally upregulates  $\mu3A$  to reroute AMPAR into the RE pathway and is essential for the recruitment of AMPAR to the cell surface during synaptic scaling up (Figure S1).

## RESULTS

We set out to identify in an unbiased manner a set of candidate “scaling factors” that might participate in transcription-dependent synaptic scaling up. The ex vivo slice and profiling studies

were conducted on HsCt5 mice (described later) at postnatal day (P) 14 to P15, an age at which synaptic scaling can be induced within L4 star pyramidal neurons by 2 days of optic nerve blockade using intraocular TTX (Figure 1A; Desai et al., 2002). In vitro experiments were performed on postnatal visual cortical cultures after 7–8 days in vitro, and pyramidal neurons were targeted using standard morphological features as described (Watt et al., 2000).

### Generation and Characterization of the HsCt5 Mouse

The HsCt5 mouse was generated as part of a lentiviral enhancer trap screen (Kelsch et al., 2012; Shima et al., 2016) through random insertion of a lentiviral vector containing the tet-transactivator (tTA) driving mCitrine. Upon screening lines for restricted mCitrine expression, the HsCt5 line was identified as having expression largely restricted to neocortical L4 (Figure 1B; Figure S2A). For many labeled neurons in V1, a thin apical dendrite could be discerned (Figure S2B), as is typical of star pyramidal neurons (Desai et al., 2002; Maffei et al., 2004). When slices were fixed and stained against  $\gamma$ -aminobutyric acid (GABA; Figures S2B and S2C) 97.5% of mCitrine<sup>+</sup> neurons were GABA negative ( $n = 685$  cells from three animals). Whole-cell current clamp recordings from labeled neurons in slices from V1 revealed that recorded neurons had regular-spiking properties, and fills revealed the typical star-pyramid morphology (Figure 1C,  $n = 5$ ). Thus, most labeled neurons were excitatory star pyramidal neurons.

Next, we verified that excitatory synapses onto labeled neurons undergo synaptic scaling up upon visual deprivation. We used an established protocol (Desai et al., 2002; Maffei and Turrigiano, 2008) to block optic nerve impulses with intraocular TTX injections for 2 days commencing just before eye opening (~P12; Figure 1A). Only one optic nerve was blocked, allowing us to use the contralateral monocular V1 from the same animals as a control. Slice recordings were then obtained from mCitrine<sup>+</sup> neurons in either the deprived or the control hemisphere, and AMPAR-mediated mEPSCs measured as described previously (Figure 1D; Desai et al., 2002; Maffei and Turrigiano, 2008). Consistent with our previous findings in rats (Desai et al., 2002), 2 days of optic nerve block significantly increased mEPSC amplitude in mCitrine<sup>+</sup> neurons (Figures 1E and 1F,  $n = 11$  each condition,  $p = 0.015$ ) without affecting mEPSC frequency ( $p = 0.17$ ), mEPSC kinetics (rise and decay times,  $p > 0.29$ ; Figure 1F, peak-scaled mEPSC waveforms), or passive cellular properties ( $R_{in}$ , input resistance;  $V_m$ , resting membrane potential; membrane capacitance,  $C_m$ ;  $p > 0.05$ ). Furthermore, mEPSC amplitude was scaled up multiplicatively (Figure 1E), as is characteristic of synaptic scaling both in vitro (Turrigiano et al., 1998) and in vivo at this developmental stage (Desai et al., 2002; Goel and Lee, 2007).

### Microarray Screen for the Synaptic-Scaling-Associated Transcriptome

To probe for candidate synaptic scaling factors with expression levels persistently and significantly altered by visual deprivation, we used the same deprivation paradigm described earlier (Figure 1A) and then isolated the monocular portion of V1 from both the deprived and the control hemispheres. L4 mCitrine<sup>+</sup>

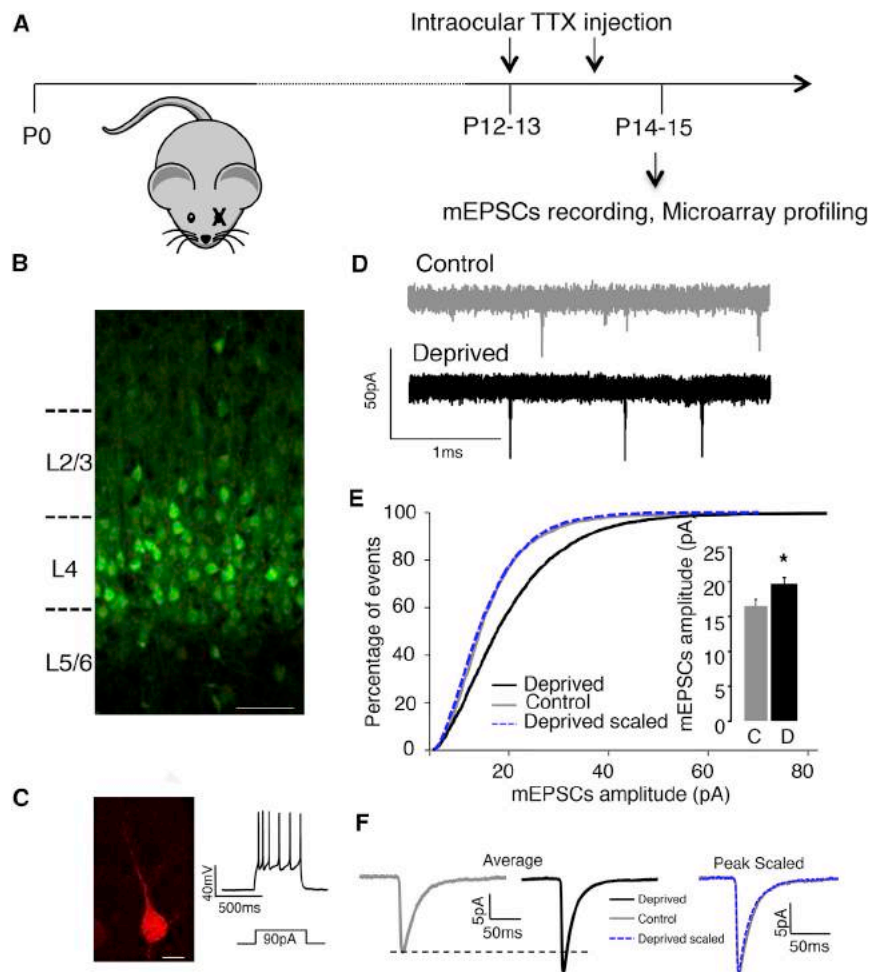


**Figure 1. Characterization of Synaptic Scaling in L4 Star Pyramidal Neurons in the HsCt5 Mouse**

(A) Visual deprivation paradigm. (B) Coronal section from the HsCt5 mouse at P15, showing mCitrine<sup>+</sup> neurons (green) in V1. Scale bar, 50  $\mu$ m. (C) Recordings from L4 mCitrine<sup>+</sup> neurons at P15. Fill during current clamp recording (left) and examples of evoked firing (right). (D) Representative mEPSC recordings from control and deprived mCitrine<sup>+</sup> neurons in L4 V1. (E) Cumulative mEPSC amplitude distributions for control and deprived conditions; the dashed line shows scaled-down amplitude distribution. Inset: average mEPSC amplitudes. (F) Average mEPSC waveforms (left) and peak-scaled mEPSC waveforms (right) to illustrate average kinetics. \* $p < 0.05$  indicates different from control; \*\* $p < 0.01$ ; sample sizes are given in the text. All summary data are expressed as mean  $\pm$  SEM. See also Figure S2.

rigiano, 2012), did not reach the criterion for altered expression (Table S1).

None of the top differentially expressed transcripts have previously been implicated in synaptic scaling. These include *Ptpn11* (a protein tyrosine phosphatase), *Map3k2* (a member of the mitogen-activated protein [MAP] kinase pathway), and *Dbp* (the clock gene D site albumin promoter binding protein; Table 1). There were several transcripts involved in ubiquitin processing, including *Ube2g1* (a

cells were isolated and manually sorted, and their mRNA was linearly amplified and used to probe affymetrix microarrays as previously described (see Experimental Procedures; Sugino et al., 2006). Expression levels were then compared between the control and the deprived hemisphere in three biological replicates. We identified the top 30 differentially expressed transcripts based on robust expression changes (fold change  $> 1.5$ ), ranked by  $p$  value (Table 1).

None of the classic activity-regulated genes (such as *c-Fos*, *Arc*, *BDNF*, or *Npas1-4*; Flavell and Greenberg, 2008), some of which (BDNF and *Arc*) have previously been implicated in synaptic scaling (Shepherd et al., 2006; Rial Verde et al., 2006; Rutherford et al., 1998), showed changes in expression that reached the criterion, likely because the manipulation we used here (2 days of optic nerve block) is subtle relative to classic activity deprivation or enhancement paradigms, such as prolonged enucleation and dark rearing or high K<sup>+</sup> and seizure induction (Flavell and Greenberg, 2008; Nedivi et al., 1993). There was also no change in expression of AMPAR or other glutamate receptor subunits. Finally, transcripts coding for a number of trafficking proteins, regulatory proteins, and kinases previously implicated in synaptic scaling (including GRIP1, PICK1, Homer1, PSD-95, Narp1, Plk2, CDK5, DHHC2, CaMKIV, and MeCP2; Tur-

ubiquitin-conjugating enzyme), *Usp48* (a predicted but uncharacterized ubiquitin peptidase), and *Anapc1* (anaphase promoting complex 1, a member of a large E3 ubiquitin ligase complex), and several with known or putative involvement in protein trafficking, including *Dync2h1* (cytoplasmic dynein 2 heavy chain 1), *Dlg1* (the trafficking/scaffold protein SAP97), and *Ap3m1* and *Ap4m* ( $\mu$  subunits of the tetrameric clathrin adaptor protein complex, or APC, family members AP-3 and AP-4). The two most significant hits in this group were *Ap3m1* (coding for  $\mu$ 3A) and *Ap4m* (coding for  $\mu$ 4), which increased 2.9- and 2.2-fold, respectively (Table 1). None of the other AP-3 or AP-4 subunits showed altered expression, and a second isoform of *Ap3m*, *Ap3m2* (coding for  $\mu$ 3B), was unaffected.

To determine whether these expression changes were predictive of increased protein levels during synaptic scaling, we analyzed a subset of these hits using quantitative immunohistochemistry in vitro (Figure 2; Figure S6A). We treated neocortical cultures with TTX for 6 hr (a period sufficient to induce transcription-dependent scaling up in vitro; Ibatata et al., 2008; Gainey et al., 2015); fixed, permeabilized, and stained against SAP97,  $\mu$ 3, or profilin 1; and then quantified the intensity of the signal within the somatic and dendritic compartments of morphologically identified pyramidal neurons as described (Figure 2; see

**Table 1. L4 Pyramidal Neuron Genes with Significantly Altered Expression during Synaptic Scaling**

Gene Symbol	Fold Change	p Value	Gene Name and Description	Function or Pathway
<b>Upregulated during Scaling</b>				
<i>Ube2g1</i> <sup>a</sup>	60	0.0001	ubiquitin-conjugating enzyme E2G 1	Ub
<i>Ap3m1</i>	2.9	0.0004	clathrin adaptor-related protein complex 3, $\mu$ A subunit	A
<i>Ap4m</i>	2.2	0.0005	clathrin adaptor-related protein complex 4, $\mu$ subunit	A
<i>Usp48</i>	1.9	0.0002	ubiquitin-specific peptidase 48	Ub
<i>Sic7A</i>	1.8	0.0003	solute carrier family 7 (cationic amino acid transporter)	T
<i>Arh</i>	2.1	0.0007	Aryl-hydrocarbon receptor	St
<i>Cacnb1</i>	1.9	0.0011	calcium channel, voltage dependent, $\beta$ 1 subunit	–
<i>Ptpnj</i>	3.0	0.0012	protein tyrosine phosphatase, receptor type, J	K/P
<i>Dlg1</i> <sup>a</sup>	17.4	0.0013	disks, large homolog 1 (SAP97)	–
<i>Nyap2</i>	2.8	0.0016	neuronal tyrosine-phosphorylated phosphoinositide 3-kinase adaptor 2	K/P
<i>PyCard</i>	3.5	0.0017	PYD and CARD domain containing	–
<i>Mtmr15</i>	1.9	0.0018	myotubularin-related protein 15	K/P
<i>Apbh</i>	1.7	0.0019	androgen-binding protein beta	St
<i>Tbrg1</i>	6.2	0.0021	transforming growth factor $\beta$ -regulated gene 1/NIAM	–
<i>Pfn1</i>	2.1	0.0022	profilin 1	–
<i>Pggt1b</i>	3.3	0.0022	protein geranylgeranyltransferase type I, $\beta$ subunit	–
<i>Hsd12</i>	5.6	0.0023	hydroxysteroid dehydrogenase-like 2	St
<i>Abcc1</i>	1.5	0.0023	ATP-binding cassette, subfamily C (CFTR/MRP), member 1	T
<i>Dph3</i>	2.5	0.0024	DPH3 homolog	–
<i>Olf138</i>	1.7	0.0026	olfactory receptor 138	–
<i>Rhbdd2</i>	3.8	0.0026	rhomboid domain containing 2	–
<i>Arfgef1</i>	20	0.0026	ADP-ribosylation factor guanine nucleotide-exchange factor 1	–
<i>Map3k2</i>	2.8	0.0027	mitogen-activated protein kinase kinase kinase 2	K/P
<i>Dbp</i>	2.1	0.0030	D site albumin promoter binding protein	–
<b>Downregulated during Scaling</b>				
<i>Dync2h1</i>	1.7	0.0003	Dynein cytoplasmic 2 heavy chain 1	–
<i>Sgpp1</i>	2.0	0.0007	sphingosine-1-phosphate phosphatase 1	K/P
<i>Atg5</i> <sup>a</sup>	2.4	0.0011	autophagy related 5	–
<i>V1ra8</i>	2.0	0.0015	vomer nasal 1 receptor, A8	–
<i>Anapc1</i> <sup>a</sup>	2.1	0.0021	anaphase promoting complex 1 (E3 ubiquitin ligase complex)	Ub
<i>Tceb1</i>	1.5	0.0034	transcription elongation factor B	–

A, clathrin adaptor protein complex family; Ub, ubiquitin pathway; St, steroid response; K/P, kinase or phosphatase; T, transporter.

<sup>a</sup>Intronic probe set. See also Table S1.

also Experimental Procedures; Gainey et al., 2015). Because there were no reliable commercially available antibodies against  $\mu$ 3 that worked for immunohistochemistry, we generated and characterized a  $\mu$ 3 rabbit polyclonal antibody (see also Experimental Procedures; Figure S3). There is ~80% homology between  $\mu$ 3A and  $\mu$ 3B (Pevsner et al., 1994), so this antibody recognizes both  $\mu$ 3 subunits but does not recognize other  $\mu$  subunits, such as  $\mu$ 4 (Figure S3B). SAP97 (Figures 2A–2C, n = 10–24 neurons/condition) and  $\mu$ 3 (Figures 2D and 2E, n = 16–23 neurons/condition) increased in a transcription-dependent manner within pyramidal neuronal dendrites (Figures 2B and 2E) and somata (Figure 2C) following TTX treatment. Another means of inducing synaptic scaling up is to express a dominant-negative form of CaMKIV in pyramidal neurons (Ibata et al., 2008; Pratt et al., 2011). Like TTX treatment, this significantly increased  $\mu$ 3 protein in pyramidal neuron dendrites (Figure 2F, n = 11–13 neu-

rons/condition, p < 0.04). In contrast, the profilin 1 signal was not significantly elevated by 6 hr TTX treatment (p > 0.07); thus, two of the three hits tested showed rapid upregulation at the protein level during synaptic scaling.

AP-3A is a heterotetrameric complex. To determine whether other subunits increased in tandem with  $\mu$ 3, we double-labeled against  $\mu$ 3 and the  $\delta$  subunit  $\delta$ 3, which is obligatory for full AP-3 complex formation (Kantheti et al., 1998; Peden et al., 2002). Both antibodies recognized endosomal compartments within the soma and dendrites, and ~50% of  $\delta$ 3 dendritic puncta had detectable levels of colocalized  $\mu$ 3 (Figure 2G). Although TTX increased both total  $\mu$ 3 (Figure 2H) and  $\mu$ 3 at colocalized sites (Figure 2I, p < 0.05), neither total  $\delta$ 3 nor colocalized  $\delta$ 3 were elevated by TTX (Figures 2H and 2I, n = 17–20 neurons/condition). Thus, consistent with our microarray data, synaptic scaling is associated with a selective increase in the  $\mu$ 3 protein with no

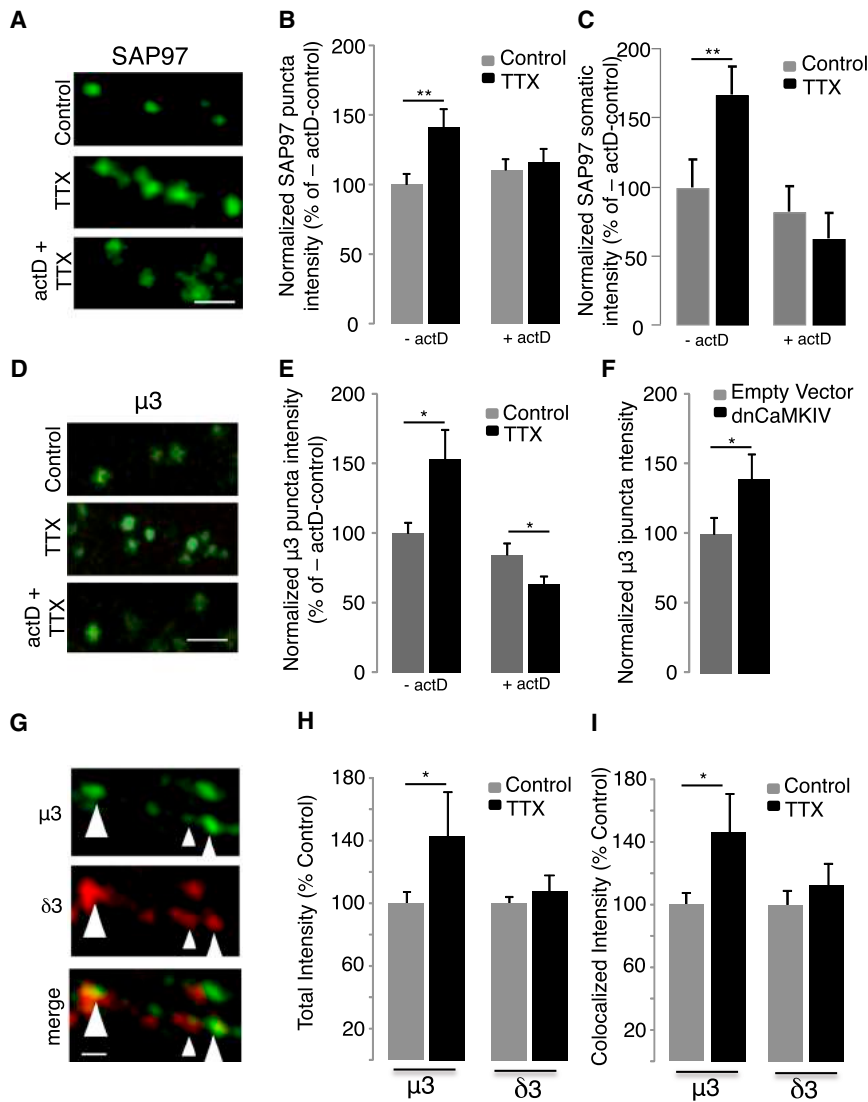


**Figure 2. Activity Deprivation In Vitro Increases SAP97 and  $\mu$ 3 Protein in Pyramidal Neurons**

(A) Examples of pyramidal neuron dendrites stained against endogenous SAP97 in control, 6 hr TTX, or 6 hr TTX + ActD treated cultures. Scale bar, 3  $\mu$ m. (B) Intensity of the punctate SAP97 signal in the dendrites for conditions in (A). (C) Total intensity of the SAP97 signal from pyramidal neuron somata. (D) Examples of cultured pyramidal neuron dendrites stained against endogenous  $\mu$ 3 in control, 6 hr TTX, or 6 hr TTX + ActD. Scale bar, 5  $\mu$ m. (E) Intensity of the punctate  $\mu$ 3 signal for conditions in (D). (F) Total intensity of the dendritic  $\mu$ 3 signal for EV and dnCaMKIV. (G) Example of the dendritic double-label against  $\mu$ 3 and  $\delta$ 3. Scale bar, 2  $\mu$ m. (H and I) Quantification of puncta intensity for all  $\mu$ 3 and  $\delta$ 3 dendritic puncta (H) and for colocalized puncta (I) following TTX treatment. \* $p < 0.05$  indicates different from control; \*\* $p < 0.01$ ; sample sizes are given in the text. All summary data are expressed as mean  $\pm$  SEM. See also Figure S3 for  $\mu$ 3 antibody characterization.

change in  $\delta$ 3. Furthermore, a significant fraction of endosomal compartments contains detectable  $\mu$ 3 without detectable  $\delta$ 3 (Figure 2G).

### Synaptic Scaling Changes the Endosomal Distribution of $\mu$ 3

AP-3A, which associates indirectly with AMPAR through  $\mu$ 3A binding to TARPs, has been implicated in the sorting and trafficking of glutamate receptors (Matsuda et al., 2013), suggesting that transcriptional upregulation of  $\mu$ 3A might play a critical role in synaptic scaling. As expected, immunohistochemistry localized  $\mu$ 3 to a number of endosomal compartments within pyramidal neurons (Figures 3A–3F), including a subset of those labeled with internalized transferrin receptor (TfR, a marker of RE), EEA1 (a marker of EEs), and LAMP1 (a lysosomal marker).

To determine whether TTX increases the accumulation of  $\mu$ 3 within specific endosomal compartments, we performed double-labeling against  $\mu$ 3 and LAMP1 (lysosomes), TfR (RE),

or EEA1 (EE) and quantified the intensity of the  $\mu$ 3 signal at colocalized sites. The  $\mu$ 3 signal associated with RE and EE was unchanged in the cell body but was significantly elevated in the dendrites (Figures 3G and 3H,  $n = 9$ –11 neurons/condition,  $p = 0.007$  RE,  $p = 0.017$  EE). In contrast, the  $\mu$ 3 signal associated with the lysosomal compartment decreased following TTX treatment in the cell body (Figure 3I,  $n = 9$ –14 neurons/condition,  $p < 0.01$ ). Thus, TTX reduces the association of  $\mu$ 3 with lysosomes while increasing its association with dendritic RE and EE.

TTX did not significantly affect the colocalization rates between  $\mu$ 3 and these various endosomal markers (data not shown). As a control, we verified that the experimental colocalization rate between  $\mu$ 3 and TfR is significantly higher than expected if the distribution of  $\mu$ 3 were random relative to the TfR signal, as described (Gainey et al., 2015); we ran the same control for triple colocalization among GluA2,  $\mu$ 3, and TfR and found that the observed rates were many fold higher than predicted for random association (Figure S4).

### Upregulation of $\mu$ 3A Is Necessary for Synaptic Scaling

To determine whether  $\mu$ 3A is necessary for synaptic scaling up, we designed two small hairpin RNAs (shRNAs) targeted against two distinct and unique regions of the  $\mu$ 3A mRNA to knock down expression of  $\mu$ 3A, an approach that allowed us to target  $\mu$ 3A in an acute and cell-autonomous manner, thus avoiding circuit level and developmental defects due to prolonged loss of  $\mu$ 3A. Neurons were transfected with the hairpins

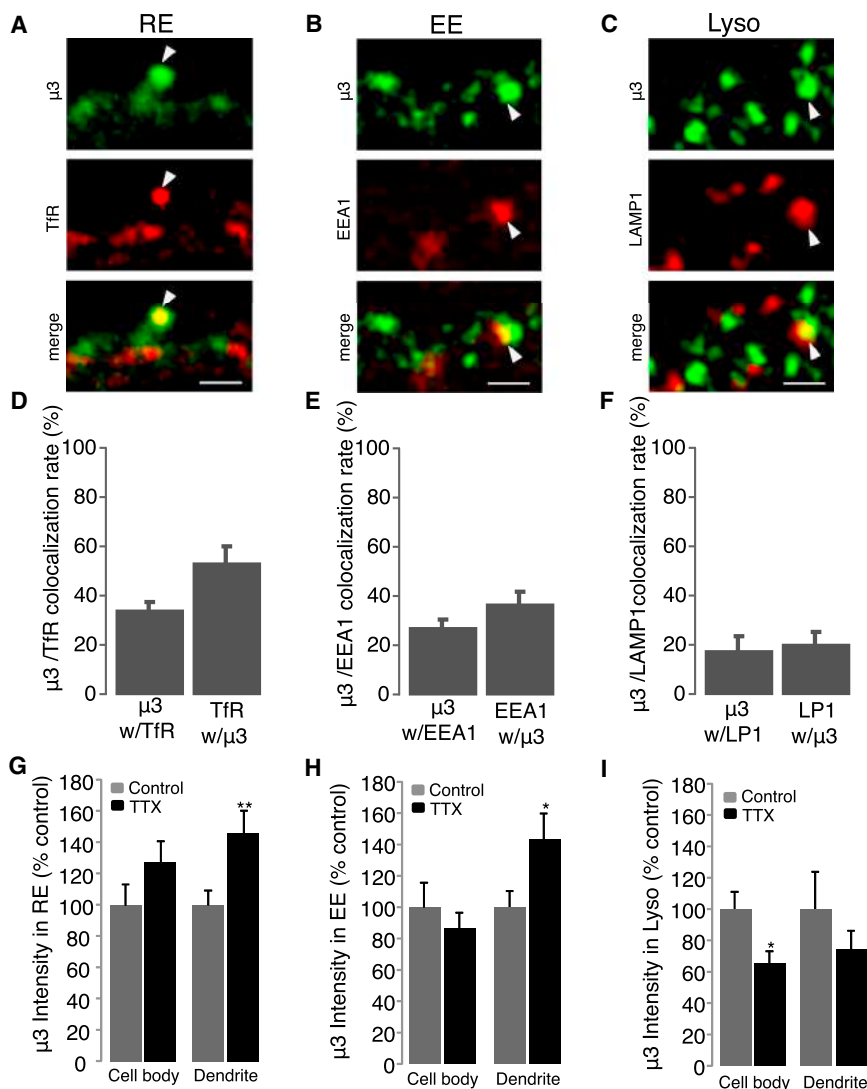


**Figure 3. Activity Deprivation Alters the Endosomal Distribution of  $\mu 3$  within Pyramidal Neuron Dendrites**

(A–C) Examples of staining in pyramidal dendrites against endogenous  $\mu 3$  (green) and (A) transferrin-labeled RE (TfR, red); (B) EE (EEA1, red); and (C) lysosomes (Lyso; LAMP1, red). Arrows show examples of colocalized puncta. Scale bars, 2  $\mu\text{m}$ . (D–F) Quantification of colocalization rates between  $\mu 3$  and TfR (D), EEA1 (E), and LAMP1 (F). (G–I) Intensity of  $\mu 3$  puncta in either the cell body or the dendrites for  $\mu 3$  puncta colocalized with TfR in RE (G), with EEA1 in EE (H), and with LAMP1 in lysosomes (I) for control and TTX-treated neurons. \* $p < 0.05$  indicates different from control; \*\* $p < 0.01$ ; sample sizes are given in the text. All summary data are expressed as mean  $\pm$  SEM.

baseline mEPSC amplitude (Figure 4E, ANOVA,  $p = 0.61$ ) or frequency (ANOVA,  $p = 0.79$ ).

Synaptic scaling in neocortical pyramidal neurons operates primarily through changes in synaptic accumulation of AMPAR (Turrigiano, 2008), so we next examined the ability of  $\mu 3\text{A}$  KD to prevent the TTX-induced enhancement of surface AMPAR. The intensity of the surface punctate GluA2 signal was increased by TTX treatment as expected (Figures 4F and 4G,  $n = 9\text{--}12$  neurons/condition,  $p = 0.04$ ), and this increase was completely blocked by  $\mu 3\text{A}$  KD (Figure 4G,  $\text{sh}\mu 3\text{A}\#1$ ); similar results were obtained with GluA1 (data not shown). Finally, coexpression of an RNAi-insensitive  $\mu 3\text{A}$  ( $\mu 3\text{AshR}$ ) was able to rescue the effects of endogenous  $\mu 3\text{A}$  KD (4G,  $\text{sh}\mu 3\text{A}\#1 + \mu 3\text{AshR}$ ); together with our

or an empty vector (EV), along with EGFP at low efficiency (Figure S6) for 3 days, and then fixed, stained, and processed for immunohistochemistry against  $\mu 3$ . Both shRNAs reduced the intensity of  $\mu 3$  staining in the somatic and dendritic compartments to  $\sim 60\%$  and  $\sim 40\%$  of control, respectively (Figures 4A and 4B,  $n = 9\text{--}13$  neurons/condition,  $p < 0.05$  for soma,  $p < 0.01$  for dendrite). This likely represents an underestimate of the degree of  $\mu 3\text{A}$  KD, because the shRNAs are specific for  $\mu 3\text{A}$  but the antibody recognizes both  $\mu 3\text{A}$  and  $\mu 3\text{B}$  (Figure S3B). Importantly, in KD neurons, TTX treatment was not able to increase  $\mu 3$  expression in either the cell body or the dendrites (Figure 4C).

Pyramidal neurons transfected with the EV showed normal synaptic scaling up of mEPSC amplitude following 6 hr TTX (Figures 4D and 4E,  $n = 12\text{--}16$  neurons/condition,  $p = 0.01$ ). In contrast, neurons in which  $\mu 3\text{A}$  had been knocked down using either shRNA, which target unique and distinct sequences in the  $\mu 3\text{A}$  mRNA, failed to show synaptic scaling up (Figures 4D and 4E,  $n = 9\text{--}11$  neurons/condition). Neither shRNA affected

earlier data using two distinct hairpins, this shows that the inability of neurons to undergo synaptic scaling is not the result of off-target effects of the shRNA.

### $\mu 3\text{A}$ Is Necessary to Traffic GluA2 to RE during Synaptic Scaling Up

The preceding data suggest that enhanced expression of  $\mu 3\text{A}$  is critical for the regulated delivery of AMPARs to synapses during synaptic scaling. AMPARs are thought to be mobilized to the dendritic surface from RE and/or EE (Park et al., 2004), and we found that dendritic  $\mu 3\text{A}$  increases in both RE and EE during synaptic scaling (Figures 3G and 3H). We thus wondered whether  $\mu 3\text{A}$  might play an important role in trafficking AMPAR to these compartments during scaling. To test this, we first asked whether  $\mu 3\text{A}$  and GluA2 are colocalized within RE and whether the amount of GluA2 at such colocalized sites is affected by TTX treatment. RE were labeled with TfR, and internal GluA2 was labeled by applying antibody to the surface, waiting 45 min for receptor internalization, stripping surface

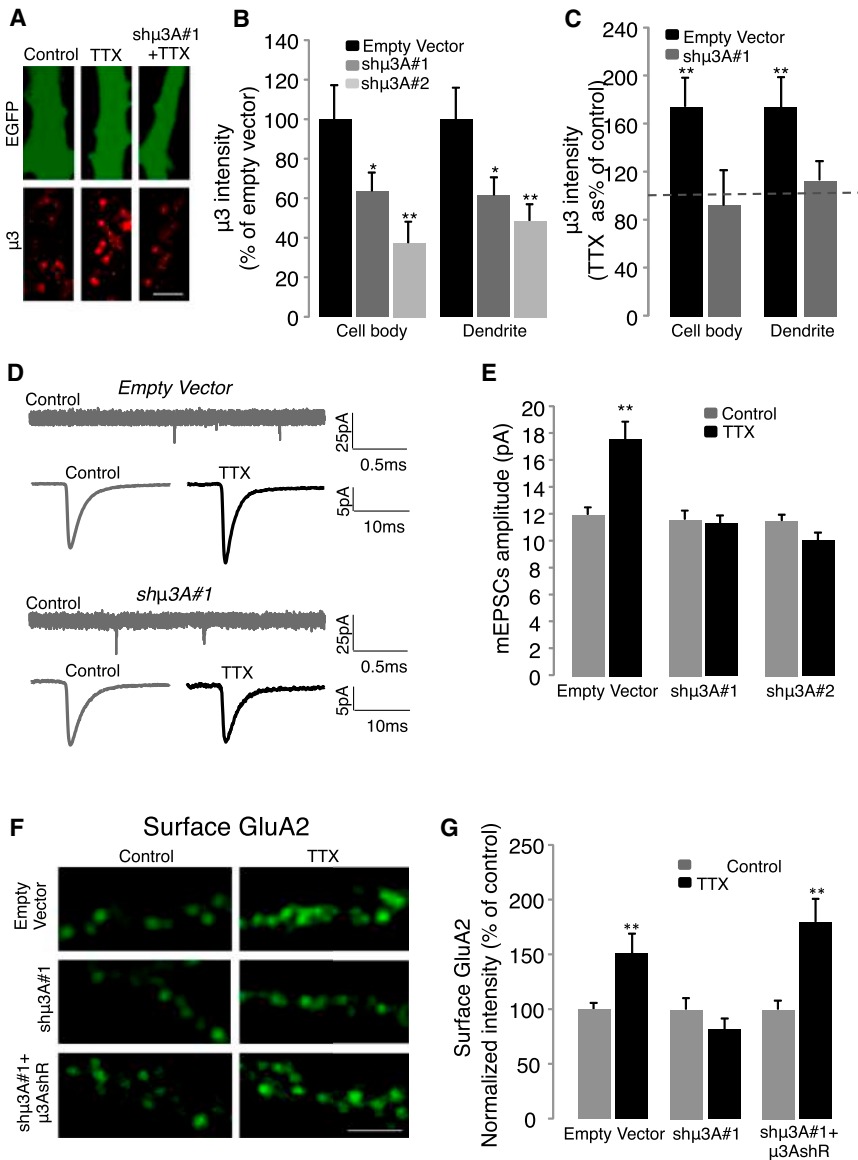


**Figure 4. KD of  $\mu$ 3A Blocks Synaptic Scaling**

(A) Example staining against endogenous  $\mu$ 3 for control and TTX-treated neurons expressing EV or the shRNA  $sh\mu$ 3A#1 in pyramidal dendrites. Scale bar, 5  $\mu$ m. (B) Quantification of the  $\mu$ 3 signal for EV,  $sh\mu$ 3A#1, and  $sh\mu$ 3A#2. (C) Quantification of the  $\mu$ 3 signal for EV or  $sh\mu$ 3A#1,  $\pm$ TTX for 6 hr. (D) Representative mEPSC recording (top trace) and average mEPSC waveforms  $\pm$  TTX (bottom traces) from EV- or  $sh\mu$ 3A#1-transfected pyramidal neurons. (E) Average mEPSC amplitude for EV-,  $sh\mu$ 3A#1-, and  $sh\mu$ 3A#2-expressing neurons,  $\pm$ TTX for 6 hr (TTX). (F) Examples of staining against endogenous surface GluA2 for neurons expressing EV or shRNA  $sh\mu$ 3A#1 or coexpressing  $sh\mu$ 3A#1 and RNAi-resistant  $\mu$ 3A ( $\mu$ 3AshR),  $\pm$ TTX for 6 hr. Scale bar, 5  $\mu$ m. (G) Quantification of the surface GluA2 signal in dendrites for the conditions in (F). \* $p < 0.05$  indicates different from control; \*\* $p < 0.01$ ; sample sizes are given in the text. All summary data are expressed as mean  $\pm$  SEM.

antibody, and then permeabilizing and staining for  $\mu$ 3 (Figure 5A; Tatavarty et al., 2013; Gainey et al., 2015). A significant fraction of internalized GluA2 puncta were colocalized with  $\mu$ 3 in RE (Figure 5B, left panel,  $\sim$ 18% in dendritic compartments), many fold higher than expected for random colocalization (Figure S4). Although TTX did not affect the fraction of RE with detectable GluA2 and  $\mu$ 3, there was a significant increase in the intensity of both the GluA2 and the  $\mu$ 3 signal within this population of dendritic RE following TTX treatment (Figures 5C and 5D,  $n = 12$ –13 neurons/condition). Thus, TTX treatment simultaneously enhances the accumulation of GluA2 and  $\mu$ 3 within a subset of dendritic RE.

Next, we asked whether this TTX-induced enhancement of GluA2 in RE depends on  $\mu$ 3A. Neurons were transfected with either EV or  $sh\mu$ 3A, and internal GluA2 in RE was labeled as earlier (Figure 6A). In the EV condition, TTX treatment

increased the intensity of the GluA2 signal within the RE compartment, and this increase was completely blocked by KD of  $\mu$ 3A (Figures 6B and 6C). This demonstrates that the deprivation-induced increase in  $\mu$ 3A is necessary for enhanced trafficking of GluA2-containing AMPAR to RE. Interestingly, KD of  $\mu$ 3A did not significantly affect basal levels of internal GluA2 (Figure 6C,  $n = 12$  neurons/condition,  $p = 0.40$ , compare EV to  $sh\mu$ 3A), suggesting that the ability of  $\mu$ 3A KD to prevent the TTX-induced enhancement of surface GluA2 does not result from a gross defect in basal trafficking of GluA2 to RE.

To determine whether upregulation of  $\mu$ 3A was sufficient to drive GluA2 to RE, we OE FLAG tagged  $\mu$ 3A and quantified the GluA2 signal within RE as earlier. OE of  $\mu$ 3A significantly increased the intensity of the GluA2 signal within RE (Figure 6D, EV,  $n = 46$ ;  $\mu$ 3A,  $n = 43$ ,  $p = 0.014$ ). In contrast,  $\mu$ 3A OE did not affect the intensity of the GluA2 signal within other endosomal compartments (Figures S6B and S6C). Next, we asked whether  $\mu$ 3A must interact with the AP-3 complex to traffic GluA2 to RE. The  $\mu$ 3A subunit interacts with the AP-3A complex through its N-terminal domain and interacts with TARPs (and thus AMPAR) through its C-terminal domain (Aguilar et al., 1997; Mardones et al., 2013; Matsuda et al., 2013). Because TTX selectively increases  $\mu$ 3A without increasing expression of the other AP-3 subunits, and OE of  $\mu$ 3A alone is sufficient to recruit AMPAR to RE (Figure 6D), we reasoned that  $\mu$ 3A might be acting independently of the full AP-3 complex during synaptic scaling. To test



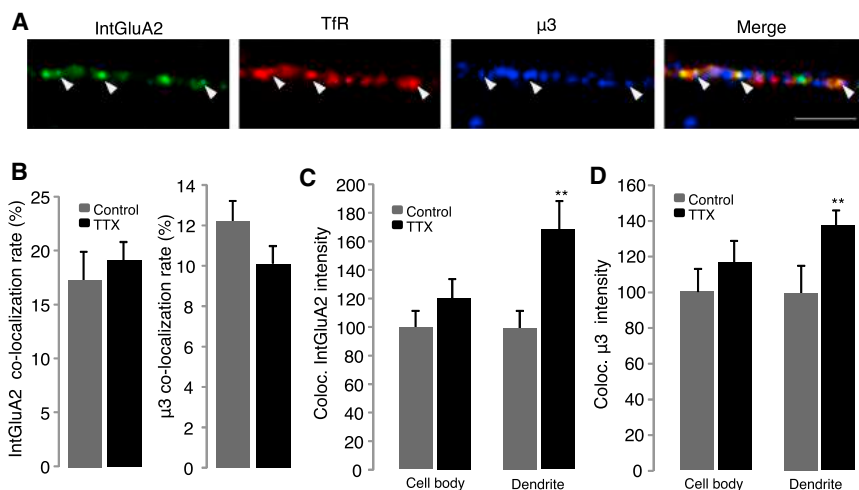


**Figure 5. Activity Blockade Increases the Abundance of GluA2 in  $\mu$ 3-Containing RE**

(A) Example images of dendritic labeling for endogenous internalized GluA2 (IntGluA2, green), TfR-labeled RE (red), and endogenous  $\mu$ 3 (blue). Arrows indicates example triple colocalized puncta. Scale bar, 5  $\mu$ m.

(B) Quantification of colocalization rates for IntGluA2 with  $\mu$ 3 and TfR (left) and for  $\mu$ 3 with IntGluA2 and TfR (right),  $\pm$ TTX.

(C) Quantification of IntGluA2 intensity at triple colocalized sites in the cell body or dendrites of pyramidal neurons,  $\pm$ TTX.

(D) Quantification of  $\mu$ 3 intensity at triple colocalized sites in the cell body or dendrites of pyramidal neurons,  $\pm$ TTX.

\* $p < 0.05$  indicates different from control; \*\* $p < 0.01$ ; sample sizes are given in the text. All summary data are expressed as mean  $\pm$  SEM. See also Figure S4.

this idea further, we OE a truncated form of  $\mu$ 3A that lacks the N-terminal domain but can still recognize and bind cargo (Mardones et al., 2013). This truncated  $\mu$ 3A was still able to traffic to RE (Figure S5), and like full-length  $\mu$ 3A, was able to recruit GluA2 to RE (Figure 6D,  $n = 22$ ,  $p = 0.03$ ).

If the recruitment of GluA2 to RE were sufficient to drive an increase in synaptic strength during synaptic scaling, then OE  $\mu$ 3A should increase mEPSC amplitude. To test this, neurons were transfected with EV ( $n = 8$ ), FLAG-tagged  $\mu$ 3A ( $n = 8$ ), or untagged  $\mu$ 3A ( $n = 10$ ) constructs; neither  $\mu$ 3A construct was sufficient to scale up mEPSC amplitude (Figure 6E). Thus, increased  $\mu$ 3A expression is necessary (Figures 4D and 4E) but not sufficient for the regulated recruitment of AMPAR to the synaptic membrane during synaptic scaling, suggesting that an additional trafficking step is required to bring internal AMPAR to the synaptic membrane. GRIP1 accumulates at sites of exocytosis, as well as at synapses, and is essential to recruit AMPAR to synapses during synaptic scaling up (Gainey et al., 2015; Tan et al., 2015). To determine whether the  $\mu$ 3A-dependent trafficking of GluA2 into the recycling pathway enhances the ability of GRIP1 to recruit GluA2 to the membrane, we compared surface levels of endogenous GluA2 after OE of  $\mu$ 3A alone, GRIP1 alone, or  $\mu$ 3A + GRIP1 (Figure 6F). While neither alone was sufficient to significantly increase surface GluA2, the two together produced a robust recruitment of GluA2 to the membrane (Figure 6G,  $n = 25$ – $33$  neurons/condition, ANOVA followed by post hoc Tukey test,  $p = 0.024$ ). Taken together, our data suggest a novel role for  $\mu$ 3A in which selective activity-dependent upregulation of the  $\mu$ 3A (cargo recognition) subunit reroutes AMPARs into the recycling pathway, where they can then be recruited to the membrane during a second trafficking step (Figure S1).

## DISCUSSION

To generate insight into the transcription-dependent processes that induce synaptic scaling up, we devised a cell-type-specific screen to identify a set of candidate scaling factors with altered expression during scaling. This screen identified  $\mu$ 3A, the cargo-recognition subunit of the APC family member

AP-3, as important for sorting and trafficking of membrane-bound cargo between endosomal compartments. Because of the known association of  $\mu$ 3A with AMPAR, we set out to determine whether  $\mu$ 3A has a role in the regulated changes in AMPAR trafficking that drive synaptic scaling. We found that activity blockade reroutes both  $\mu$ 3A and GluA2 into RE, without affecting the  $\delta$ 3 subunit, which is obligatory for complex formation. KD of  $\mu$ 3A prevented synaptic scaling and the redistribution of GluA2 into RE, while OE of either full-length  $\mu$ 3A or a truncated form that cannot interact with the AP-3A complex was sufficient to drive GluA2 to REs. Finally, OE of  $\mu$ 3A acted synergistically with GRIP1 to recruit GluA2 to the cell surface. Taken together, these data support a model in which excess  $\mu$ 3A acts independently of the AP-3A complex to reroute AMPAR to RE, from which they are recruited to the synapse to enhance synaptic strength during scaling up (Figure S1).

We used an unbiased cell-type-specific profiling approach (Sugino et al., 2006) that allowed us to probe for persistent transcriptional changes in a population of neurons (L4 star pyramidal neurons from V1) known to undergo synaptic scaling in response to visual deprivation during early postnatal development (Desai et al., 2002). None of the small number of candidates identified (Table 1) had previously been associated with synaptic scaling. There is no overlap between this candidate set and transcripts previously found to be regulated by visual deprivation in V1 of rodents or primates (Nedivi et al., 1996; Lachance and Chaudhuri, 2004; Majdan and Shatz, 2006; Tropea et al., 2006). This is likely due to large methodological differences in approach; most importantly, these previous studies probed whole V1 extracts, while here we probe changes in a specific cell type as these neurons are undergoing synaptic scaling. Because of the complexity of neocortical circuits and cell types and the diversity of plasticity mechanisms present (Feldman, 2009; Nelson and Turrigiano, 2008), this cell-type-specific approach is likely critical for identifying candidates that are tied to particular forms of neocortical plasticity, rather than general circuit-wide responses to deprivation or other activity paradigms.

Interestingly, none of the signaling and trafficking proteins that have previously been linked to synaptic scaling through a

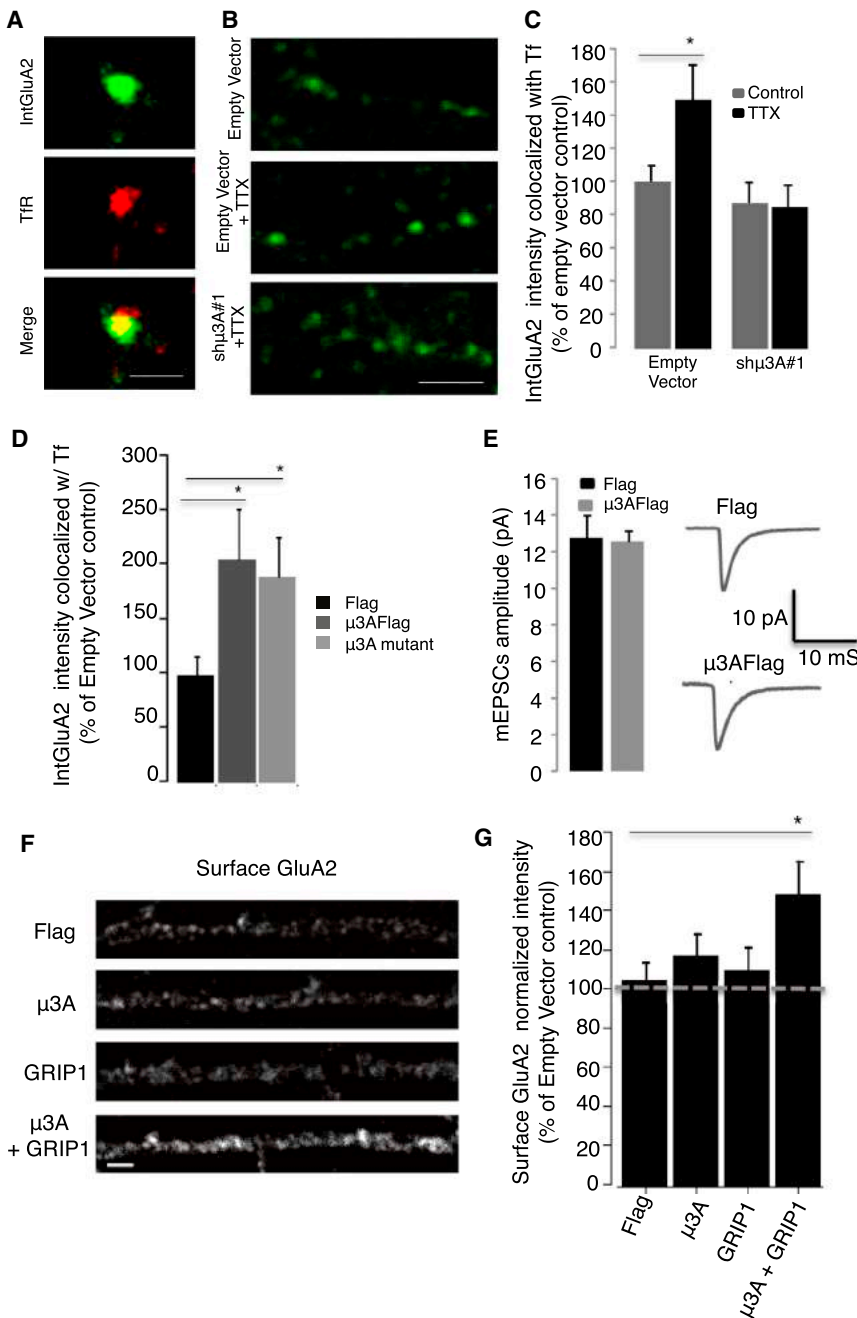


**Figure 6.  $\mu$ 3 Is Necessary and Sufficient to Recruit GluA2 to RE and Enhances the Ability of GRIP1 to Recruit GluA2 to the Dendritic Surface**

(A) Example of the internalized GluA2 signal (green) within RE (TfR, red). Scale bar, 1  $\mu$ m.

(B) Dendritic internalized GluA2 signal for EV, EV + TTX, or sh $\mu$ 3A#1 + TTX conditions. Scale bar, 5  $\mu$ m. (C) Quantification of the intensity of internalized GluA2 colocalized with TfR in pyramidal dendrites transfected with EV or sh $\mu$ 3A#1,  $\pm$  6 hr TTX.

(D) Quantification of the intensity of internalized GluA2 colocalized with TfR in pyramidal dendrites transfected with EV,  $\mu$ 3A-FLAG, or truncated  $\mu$ 3A-FLAG.

(E) Average mEPSC amplitude for FLAG or  $\mu$ 3A-FLAG-transfected pyramidal neurons.

(F) Example dendritic staining for surface GluA2 after transfection with FLAG alone,  $\mu$ 3A-FLAG, GRIP1, or  $\mu$ 3A-FLAG + GRIP1.

(G) Quantification of the conditions in (F). \* $p$  < 0.05 indicates different from control; \*\* $p$  < 0.01; sample sizes are given in the text. All summary data are expressed as mean  $\pm$  SEM. See also Figures S5 and S6.

(Matsuda et al., 2008; Bendor et al., 2010) and, more recently, AP-3A has been shown to interact with AMPAR through an indirect association involving  $\mu$ 3A binding to the TARP stargazin (STG), an association that is important for the induction of long-term depression (LTD) (Matsuda et al., 2013). None of the tetrameric APC family member subunits were previously known to exhibit activity-dependent transcriptional regulation, whereas here we find that both  $\mu$ 3A and  $\mu$ 4 (but not any other subunits of either APC) were upregulated by day 2 of visual deprivation. AP-3A is primarily known for a role in sorting cargo from the Golgi or EE to lysosomes or lysosome-related organelles (LROs) (Dell'Angelica, 2009; Dell'Angelica et al., 1997; Peden et al., 2004), and during LTD, the association of  $\mu$ 3A with stargazin enhances the trafficking of AMPAR to lysosomes (Matsuda et al., 2013). Thus, it

candidate approach came up in our screen (Table S1). As an example, the essential scaling factor GRIP1 is not transcriptionally regulated, consistent with the observation that although GRIP1 increases at synapses during scaling, this is not accompanied by an increase in total GRIP1 protein (Gainey et al., 2015). This underscores the point that synaptic scaling involves the activity-dependent regulation of several AMPAR trafficking steps, only some of which are regulated at the level of transcription.

We chose to focus on  $\mu$ 3A because AP-3 plays a role in trafficking of receptors into dendrites and/or to the neuronal surface

was a surprise to find that during synaptic scaling, the upregulation of  $\mu$ 3A leads to enhanced accumulation of  $\mu$ 3A and AMPAR within the RE compartment and a reduction in the association of  $\mu$ 3A with lysosomes. These data show that the localization of  $\mu$ 3A is dynamic and can be regulated by activity to redirect cargo (in particular, AMPAR) into the recycling endocytic pathway.

The RE compartment has been shown to be critical for supplying AMPAR during LTP (Hanley, 2010; Park et al., 2004), but whether they also supply AMPAR for synaptic scaling has been less clear (Gainey et al., 2015; Tan et al., 2015). Interestingly, although an increase in  $\mu$ 3A is necessary for scaling, and

is necessary and sufficient to drive AMPAR to RE, it is not sufficient to increase mEPSC amplitude. This suggests that once AMPAR are rerouted into the recycling pathway by  $\mu$ 3A, they must still be recruited to the synaptic membrane in a second activity-dependent trafficking step. The GluA2-interacting protein GRIP1 plays a critical role in recruiting AMPAR from internal endosomal compartments to the synaptic membrane during synaptic scaling (Gainey et al., 2015; Tan et al., 2015). Here we show that when  $\mu$ 3A and GRIP1 are OE together, they can act synergistically to enhance surface AMPAR accumulation, providing direct experimental support for a two-step trafficking model in which  $\mu$ 3A recruits AMPAR into the recycling pathway, where they can then be recruited to and stabilized by GRIP1 at the synaptic membrane (Figure S1).

Systemic loss of functional AP-3 causes endosomal trafficking defects, Hermansky-Pudlak syndrome, and neurological symptoms (Kantheti et al., 1998; Lane and Deol, 1974; Peden et al., 2002; Seong et al., 2005; Sirkis et al., 2013; Swank et al., 2000; Yang et al., 2000). These have mainly been ascribed to defects in lysosomal trafficking and/or biogenesis of LROs. Our data suggest that the  $\mu$ 3A subunit traffics AMPAR away from lysosomes and into the recycling pathway by acting independently of the full AP-3 complex. Three main pieces of evidence support this idea. First, while  $\mu$ 3A is upregulated during synaptic scaling, the  $\delta$ 3 subunit is not. Because the  $\delta$ 3 subunit is obligatory for formation of both the AP-3A and the AP-3B complexes (Kantheti et al., 1998; Peden et al., 2002), this suggests that either  $\mu$ 3A is limiting for complex formation or that activity-induced  $\mu$ 3A is not acting as part of the complex. The latter interpretation is favored by the observation that the intensity of the  $\mu$ 3A signal increases even in endosomal compartments with no detectible  $\delta$ 3. Second, we find that OE of  $\mu$ 3A alone is sufficient to recruit AMPAR to RE and to enhance the ability of GRIP1 to recruit AMPAR to the dendritic membrane. Finally, OE of a truncated  $\mu$ 3A that cannot interact with the AP-3 complex is also able to recruit AMPAR to RE. These data show that selectively increasing  $\mu$ 3A is able redirect AMPAR into the recycling pathway, possibly by protecting AMPAR from association with the full AP-3 complex. Once in the recycling pathway, they can be recruited to the synapse during a subsequent trafficking step, likely involving GRIP1 (Figure S1).

Taken together, our data identify  $\mu$ 3A as an essential transcription-dependent switch point that can redirect AMPAR to RE during synaptic scaling. These data show that both scaling up and LTP share a common reliance on AMPAR trafficking to the RE compartment (Ehlers, 2000; Park et al., 2004). Furthermore, AP-3 is important for trafficking AMPAR to lysosomes during LTD (Matsuda et al., 2013). This raises the possibility that competition between AP-3 and  $\mu$ 3A for the binding and sorting of AMPAR is a key mechanism underlying several distinct forms of synaptic plasticity.

## EXPERIMENTAL PROCEDURES

All experiments were approved by the Brandeis Animal Care and Use Committee and were in accordance with NIH guidelines. Experiments were performed on animals of both sexes. Detailed methods are provided in [Supplemental Experimental Procedures](#). Briefly, cultures were prepared and transfected

72 hr before recording or staining as described (Pratt et al., 2003). For culture physiology, mEPSC recordings were obtained from visually identified pyramidal neurons and analyzed as described previously (Turrigiano et al., 1998; Wierenga et al., 2005). At P12 or P13, HsCt5 mice were subjected to monocular deprivation by intraocular injection of TTX (1 mM) as described (Desai et al., 2002; Maffei and Turrigiano, 2008); injections were performed twice (at P12 or P13 and then again at P13 or P14) to maintain the block for 48 hr. For slice electrophysiology, coronal brain slices from HsCt5 mice (300  $\mu$ m) containing monocular primary visual cortex (V1m) were prepared from control and deprived hemispheres (P14–P15) and recordings were obtained from labeled neurons as described (Maffei et al., 2006; Loebrich et al., 2013).

## Microarray Screen

Isolation of labeled neurons, RNA preparation, and microarray screening from L4 V1 from the HsCt5 line was performed as described previously (Suginio et al., 2006; Hempel et al., 2007), using 30 to 50 labeled cells from either the deprived or the control hemisphere for each of three replicates. To stabilize the probe effects (i.e., probe-specific sources of variance), we used an approach similar to the frozen robust multiarray analysis (fRMA) method developed by McCall et al. (2010); details are given in [Supplemental Experimental Procedures](#). Data were filtered by fold change > 1.5, and the top 30 probes (ranked by p value) annotated to RefSeq genes were included in Table 1.

## Antibody Generation and Characterization

A rabbit anti- $\mu$ 3 polyclonal antibody was raised against the peptide DMYGEK YKPFKGVKY (LifeTein, residues 393–407) by Cocalico Biologicals. Bleeds were examined and specificity was confirmed by western blot analysis against cortical extracts, and 293 lysates (ATCC) transfected with *Ap3m1*, *Ap3m2*, or *Ap4m1*-mCherry expression vectors. Immunohistochemical staining was abolished by preabsorption with the peptide used to generate the antibody (Figure S3C) and was decreased when  $\mu$ 3A was knocked down by RNAi (Figures 4A–4C).

## Statistical Analysis

Data are presented as mean  $\pm$  SEM for the number of neurons indicated. Each experiment was repeated on at least three separate animals or dissociations, and the n values represent the number of neurons. To determine statistical significance, unpaired two-tailed Student's t tests—or, for multiple comparisons, single-factor ANOVAs followed by a Tukey test or a Kruskal-Wallis test followed by a Dunn-Bonferroni post hoc test—were run as appropriate. p values  $\leq$  0.05 were considered significant.

## ACCESSION NUMBERS

The accession number for the data reported in this paper is GEO: GSE56758.

## SUPPLEMENTAL INFORMATION

Supplemental Information includes Supplemental Experimental Procedures, six figures, and one table and can be found with this article online at <http://dx.doi.org/10.1016/j.celrep.2016.08.009>.

## AUTHOR CONTRIBUTIONS

All authors designed or performed the experiments. C.C.S., V.T., K.S., H.L., M.L., A.J., S.B.N., and G.G.T. analyzed the data. G.G.T., C.C.S., and S.B.N. wrote the manuscript.

## ACKNOWLEDGMENTS

We thank Lirong Wang, Saori Kato, Alina Chima, Dan Acker, Aram Raissi, and Zhe Meng for technical assistance. This study was supported by R37 NS092635 (G.G.T.), R01EY022360 (S.B.N.), and PO1 NS079419 (G.G.T. and S.B.N.).

Received: April 12, 2014  
 Revised: July 15, 2016  
 Accepted: August 1, 2016  
 Published: August 25, 2016

## REFERENCES

- Aguilar, R.C., Ohno, H., Roche, K.W., and Bonifacino, J.S. (1997). Functional domain mapping of the clathrin-associated adaptor medium chains mu1 and mu2. *J. Biol. Chem.* *272*, 27160–27166.
- Bendor, J., Lizardi-Ortiz, J.E., Westphalen, R.I., Brandstetter, M., Hemmings, H.C., Jr., Sulzer, D., Flajolet, M., and Greengard, P. (2010). AGAP1/AP-3-dependent endocytic recycling of M5 muscarinic receptors promotes dopamine release. *EMBO J.* *29*, 2813–2826.
- Bonifacino, J.S., and Traub, L.M. (2003). Signals for sorting of transmembrane proteins to endosomes and lysosomes. *Annu. Rev. Biochem.* *72*, 395–447.
- Davis, G.W. (2013). Homeostatic signaling and the stabilization of neural function. *Neuron* *80*, 718–728.
- Dell'Angelica, E.C. (2009). AP-3-dependent trafficking and disease: the first decade. *Curr. Opin. Cell Biol.* *21*, 552–559.
- Dell'Angelica, E.C., Ohno, H., Ooi, C.E., Rabinovich, E., Roche, K.W., and Bonifacino, J.S. (1997). AP-3: an adaptor-like protein complex with ubiquitous expression. *EMBO J.* *16*, 917–928.
- Desai, N.S., Cudmore, R.H., Nelson, S.B., and Turrigiano, G.G. (2002). Critical periods for experience-dependent synaptic scaling in visual cortex. *Nat. Neurosci.* *5*, 783–789.
- Ehlers, M.D. (2000). Reinsertion or degradation of AMPA receptors determined by activity-dependent endocytic sorting. *Neuron* *28*, 511–525.
- Faúndez, V., Horng, J.T., and Kelly, R.B. (1998). A function for the AP3 coat complex in synaptic vesicle formation from endosomes. *Cell* *93*, 423–432.
- Feldman, D.E. (2009). Synaptic mechanisms for plasticity in neocortex. *Annu. Rev. Neurosci.* *32*, 33–55.
- Flavell, S.W., and Greenberg, M.E. (2008). Signaling mechanisms linking neuronal activity to gene expression and plasticity of the nervous system. *Annu. Rev. Neurosci.* *31*, 563–590.
- Gainey, M.A., Hurvitz-Wolff, J.R., Lambo, M.E., and Turrigiano, G.G. (2009). Synaptic scaling requires the GluR2 subunit of the AMPA receptor. *J. Neurosci.* *29*, 6479–6489.
- Gainey, M.A., Tatavarty, V., Nahmani, M., Lin, H., and Turrigiano, G.G. (2015). Activity-dependent synaptic GRIP1 accumulation drives synaptic scaling up in response to action potential blockade. *Proc. Natl. Acad. Sci. USA* *112*, E3590–E3599.
- Goel, A., and Lee, H.K. (2007). Persistence of experience-induced homeostatic synaptic plasticity through adulthood in superficial layers of mouse visual cortex. *J. Neurosci.* *27*, 6692–6700.
- Goold, C.P., and Nicoll, R.A. (2010). Single-cell optogenetic excitation drives homeostatic synaptic depression. *Neuron* *68*, 512–528.
- Hanley, J.G. (2010). Endosomal sorting of AMPA receptors in hippocampal neurons. *Biochem. Soc. Trans.* *38*, 460–465.
- Hempel, C.M., Sugino, K., and Nelson, S.B. (2007). A manual method for the purification of fluorescently labeled neurons from the mammalian brain. *Nat. Protoc.* *2*, 2924–2929.
- Hengen, K.B., Lambo, M.E., Van Hooser, S.D., Katz, D.B., and Turrigiano, G.G. (2013). Firing rate homeostasis in visual cortex of freely behaving rodents. *Neuron* *80*, 335–342.
- Hengen, K.B., Torrado Pacheco, A., McGregor, J.N., Van Hooser, S.D., and Turrigiano, G.G. (2016). Neuronal firing rate homeostasis is inhibited by sleep and promoted by wake. *Cell* *165*, 180–191.
- Hirst, J., Irving, C., and Borner, G.H. (2013). Adaptor protein complexes AP-4 and AP-5: new players in endosomal trafficking and progressive spastic paraplegia. *Traffic* *14*, 153–164.
- Ibata, K., Sun, Q., and Turrigiano, G.G. (2008). Rapid synaptic scaling induced by changes in postsynaptic firing. *Neuron* *57*, 819–826.
- Kantheti, P., Qiao, X., Diaz, M.E., Peden, A.A., Meyer, G.E., Carskadon, S.L., Kapfhammer, D., Sufalko, D., Robinson, M.S., Noebels, J.L., and Burmeister, M. (1998). Mutation in AP-3 delta in the mocha mouse links endosomal transport to storage deficiency in platelets, melanosomes, and synaptic vesicles. *Neuron* *21*, 111–122.
- Kastning, K., Kukhtina, V., Kittler, J.T., Chen, G., Pechstein, A., Enders, S., Lee, S.H., Sheng, M., Yan, Z., and Haucke, V. (2007). Molecular determinants for the interaction between AMPA receptors and the clathrin adaptor complex AP-2. *Proc. Natl. Acad. Sci. USA* *104*, 2991–2996.
- Kelsch, W., Stolfi, A., and Lois, C. (2012). Genetic labeling of neuronal subsets through enhancer trapping in mice. *PLoS ONE* *7*, e38593.
- Kennedy, M.J., and Ehlers, M.D. (2006). Organelles and trafficking machinery for postsynaptic plasticity. *Annu. Rev. Neurosci.* *29*, 325–362.
- Lachance, P.E.D., and Chaudhuri, A. (2004). Microarray analysis of developmental plasticity in monkey primary visual cortex. *J. Neurochem.* *88*, 1455–1469.
- Lambo, M.E., and Turrigiano, G.G. (2013). Synaptic and intrinsic homeostatic mechanisms cooperate to increase L2/3 pyramidal neuron excitability during a late phase of critical period plasticity. *J. Neurosci.* *33*, 8810–8819.
- Lane, P.W., and Deol, M.S. (1974). Mocha, a new coat color and behavior mutation on chromosome 10 of the mouse. *J. Hered.* *65*, 362–364.
- Le Borgne, R., Alconada, A., Bauer, U., and Hoflack, B. (1998). The mammalian AP-3 adaptor-like complex mediates the intracellular transport of lysosomal membrane glycoproteins. *J. Biol. Chem.* *273*, 29451–29461.
- Lee, S.H., Liu, L., Wang, Y.T., and Sheng, M. (2002). Clathrin adaptor AP2 and NSF interact with overlapping sites of GluR2 and play distinct roles in AMPA receptor trafficking and hippocampal LTD. *Neuron* *36*, 661–674.
- Loebrich, S., Djukic, B., Tong, Z.J., Cottrell, J.R., Turrigiano, G.G., and Nedivi, E. (2013). Regulation of glutamate receptor internalization by the spine cytoskeleton is mediated by its PKA-dependent association with CPG2. *Proc. Natl. Acad. Sci. USA* *110*, E4548–E4556.
- Maffei, A., and Turrigiano, G.G. (2008). Multiple modes of network homeostasis in visual cortical layer 2/3. *J. Neurosci.* *28*, 4377–4384.
- Maffei, A., Nataraj, K., Nelson, S.B., and Turrigiano, G.G. (2006). Potentiation of cortical inhibition by visual deprivation. *Nature* *443*, 81–84.
- Maffei, A., Nelson, S.B., and Turrigiano, G.G. (2004). Selective reconfiguration of layer 4 visual cortical circuitry by visual deprivation. *Nat. Neurosci.* *7*, 1353–1359.
- Majdan, M., and Shatz, C.J. (2006). Effects of visual experience on activity-dependent gene regulation in cortex. *Nat. Neurosci.* *9*, 650–659.
- Mardones, G.A., Burgos, P.V., Lin, Y., Kloer, D.P., Magadán, J.G., Hurley, J.H., and Bonifacino, J.S. (2013). Structural basis for the recognition of tyrosine-based sorting signals by the  $\mu$ 3A subunit of the AP-3 adaptor complex. *J. Biol. Chem.* *288*, 9563–9571.
- Margeta, M.A., Wang, G.J., and Shen, K. (2009). Clathrin adaptor AP-1 complex excludes multiple postsynaptic receptors from axons in *C. elegans*. *Proc. Natl. Acad. Sci. USA* *106*, 1632–1637.
- Matsuda, S., Miura, E., Matsuda, K., Kakegawa, W., Kohda, K., Watanabe, M., and Yuzaki, M. (2008). Accumulation of AMPA receptors in autophagosomes in neuronal axons lacking adaptor protein AP-4. *Neuron* *57*, 730–745.
- Matsuda, S., Kakegawa, W., Budisantoso, T., Nomura, T., Kohda, K., and Yuzaki, M. (2013). Stargazin regulates AMPA receptor trafficking through adaptor protein complexes during long-term depression. *Nat. Commun.* *4*, 2759.
- McCall, M.N., Bolstad, B.M., and Irizarry, R.A. (2010). Frozen robust multiarray analysis (fRMA). *Biostatistics* *11*, 242–253.
- Meadows, J.P., Guzman-Karlsson, M.C., Phillips, S., Holleman, C., Posey, J.L., Day, J.J., Hablitz, J.J., and Sweatt, J.D. (2015). DNA methylation regulates neuronal glutamatergic synaptic scaling. *Sci. Signal.* *8*, ra61.
- Nakatsu, F., and Ohno, H. (2003). Adaptor protein complexes as the key regulators of protein sorting in the post-Golgi network. *Cell Struct. Funct.* *28*, 419–429.

- Nedivi, E., Hevroni, D., Naot, D., Israeli, D., and Citri, Y. (1993). Numerous candidate plasticity-related genes revealed by differential cDNA cloning. *Nature* 363, 718–722.
- Nedivi, E., Fieldust, S., Theill, L.E., and Hevron, D. (1996). A set of genes expressed in response to light in the adult cerebral cortex and regulated during development. *Proc. Natl. Acad. Sci. USA* 93, 2048–2053.
- Nelson, S.B., and Turrigiano, G.G. (2008). Strength through diversity. *Neuron* 60, 477–482.
- Newell-Litwa, K., Seong, E., Burmeister, M., and Faundez, V. (2007). Neuronal and non-neuronal functions of the AP-3 sorting machinery. *J. Cell Sci.* 120, 531–541.
- Ohno, H., Aguilar, R.C., Yeh, D., Taura, D., Saito, T., and Bonifacino, J.S. (1998). The medium subunits of adaptor complexes recognize distinct but overlapping sets of tyrosine-based sorting signals. *J. Biol. Chem.* 273, 25915–25921.
- Park, M., Penick, E.C., Edwards, J.G., Kauer, J.A., and Ehlers, M.D. (2004). Recycling endosomes supply AMPA receptors for LTP. *Science* 305, 1972–1975.
- Peden, A.A., Rudge, R.E., Lui, W.W., and Robinson, M.S. (2002). Assembly and function of AP-3 complexes in cells expressing mutant subunits. *J. Cell Biol.* 156, 327–336.
- Peden, A.A., Oorschot, V., Hesser, B.A., Austin, C.D., Scheller, R.H., and Klumperman, J. (2004). Localization of the AP-3 adaptor complex defines a novel endosomal exit site for lysosomal membrane proteins. *J. Cell Biol.* 164, 1065–1076.
- Pevsner, J., Volkmandt, W., Wong, B.R., and Scheller, R.H. (1994). Two rat homologs of clathrin-associated adaptor proteins. *Gene* 146, 279–283.
- Pozo, K., and Goda, Y. (2010). Unraveling mechanisms of homeostatic synaptic plasticity. *Neuron* 66, 337–351.
- Pratt, K.G., Watt, A.J., Griffith, L.C., Nelson, S.B., and Turrigiano, G.G. (2003). Activity-dependent remodeling of presynaptic inputs by postsynaptic expression of activated CaMKII. *Neuron* 39, 269–281.
- Pratt, K.G., Zimmerman, E.C., Cook, D.G., and Sullivan, J.M. (2011). Presenilin 1 regulates homeostatic synaptic scaling through Akt signaling. *Nat. Neurosci.* 14, 1112–1114.
- Rial Verde, E.M., Lee-Osbourne, J., Worley, P.F., Malinow, R., and Cline, H.T. (2006). Increased expression of the immediate-early gene *arc/arg3.1* reduces AMPA receptor-mediated synaptic transmission. *Neuron* 52, 461–474.
- Robinson, M.S., and Bonifacino, J.S. (2001). Adaptor-related proteins. *Curr. Opin. Cell Biol.* 13, 444–453.
- Rutherford, L.C., Nelson, S.B., and Turrigiano, G.G. (1998). BDNF has opposite effects on the quantal amplitude of pyramidal neuron and interneuron excitatory synapses. *Neuron* 21, 521–530.
- Seong, E., Wainer, B.H., Hughes, E.D., Saunders, T.L., Burmeister, M., and Faundez, V. (2005). Genetic analysis of the neuronal and ubiquitous AP-3 adaptor complexes reveals divergent functions in brain. *Mol. Biol. Cell* 16, 128–140.
- Shepherd, J.D., Rumbaugh, G., Wu, J., Chowdhury, S., Plath, N., Kuhl, D., Hugaranir, R.L., and Worley, P.F. (2006). *Arc/Arg3.1* mediates homeostatic synaptic scaling of AMPA receptors. *Neuron* 52, 475–484.
- Shima, Y., Sugino, K., Hempel, C.M., Shima, M., Taneja, P., Bullis, J.B., Mehta, S., Lois, C., and Nelson, S.B. (2016). A mammalian enhancer trap resource for discovering and manipulating neuronal cell types. *eLife* 5, e13503.
- Simpson, F., Peden, A.A., Christopoulou, L., and Robinson, M.S. (1997). Characterization of the adaptor-related protein complex, AP-3. *J. Cell Biol.* 137, 835–845.
- Sirkis, D.W., Edwards, R.H., and Asensio, C.S. (2013). Widespread dysregulation of peptide hormone release in mice lacking adaptor protein AP-3. *PLoS Genet.* 9, e1003812.
- Sugino, K., Hempel, C.M., Miller, M.N., Hattox, A.M., Shapiro, P., Wu, C., Huang, Z.J., and Nelson, S.B. (2006). Molecular taxonomy of major neuronal classes in the adult mouse forebrain. *Nat. Neurosci.* 9, 99–107.
- Swank, R.T., Novak, E.K., McGarry, M.P., Zhang, Y., Li, W., Zhang, Q., and Feng, L. (2000). Abnormal vesicular trafficking in mouse models of Herman-sky-Pudlak syndrome. *Pigment Cell Res.* 13 (Suppl 8), 59–67.
- Tan, H.L., Queenan, B.N., and Hugaranir, R.L. (2015). GRIP1 is required for homeostatic regulation of AMPAR trafficking. *Proc. Natl. Acad. Sci. USA* 112, 10026–10031.
- Tatavarty, V., Sun, Q., and Turrigiano, G.G. (2013). How to scale down post-synaptic strength. *J. Neurosci.* 33, 13179–13189.
- Traub, L.M., and Bonifacino, J.S. (2013). Cargo recognition in clathrin-mediated endocytosis. *Cold Spring Harb. Perspect. Biol.* 5, a016790.
- Tropea, D., Kreiman, G., Lyckman, A., Mukherjee, S., Yu, H., Horng, S., and Sur, M. (2006). Gene expression changes and molecular pathways mediating activity-dependent plasticity in visual cortex. *Nat. Neurosci.* 9, 660–668.
- Turrigiano, G.G. (2008). The self-tuning neuron: synaptic scaling of excitatory synapses. *Cell* 135, 422–435.
- Turrigiano, G. (2012). Homeostatic synaptic plasticity: local and global mechanisms for stabilizing neuronal function. *Cold Spring Harb. Perspect. Biol.* 4, a005736.
- Turrigiano, G.G., and Nelson, S.B. (2004). Homeostatic plasticity in the developing nervous system. *Nat. Rev. Neurosci.* 5, 97–107.
- Turrigiano, G.G., Leslie, K.R., Desai, N.S., Rutherford, L.C., and Nelson, S.B. (1998). Activity-dependent scaling of quantal amplitude in neocortical neurons. *Nature* 391, 892–896.
- Watt, A.J., van Rossum, M.C., MacLeod, K.M., Nelson, S.B., and Turrigiano, G.G. (2000). Activity coregulates quantal AMPA and NMDA currents at neocortical synapses. *Neuron* 26, 659–670.
- Wierenga, C.J., Ibata, K., and Turrigiano, G.G. (2005). Postsynaptic expression of homeostatic plasticity at neocortical synapses. *J. Neurosci.* 25, 2895–2905.
- Yang, W., Li, C., Ward, D.M., Kaplan, J., and Mansour, S.L. (2000). Defective organellar membrane protein trafficking in *Ap3b1*-deficient cells. *J. Cell Sci.* 113, 4077–4086.